Increased damping of irregular resonators

S. Russ[1,2] and B. Sapoval[2,3]
[1]*Institut für Theoretische Physik III, Universität Giessen, D-35392 Giessen, Germany*
[2]*Laboratoire de Physique de la Matière Condensée, CNRS, Ecole Polytechnique, 91128 Palaiseau, France*
[3]*Centre de Mathématiques et de leurs Applications, Ecole Normale Supérieure, 94140 Cachan, France*
(Received 5 February 2001; revised manuscript received 3 October 2001; published 28 February 2002)

It is shown that fractal drums and jagged geometry resonators may be more damped than ordinary Euclidean systems. Several damping mechanisms are examined and studied by numerical calculations. The results depend on the dissipation mechanisms but globally they increase with localization, frequency, and the irregularity of the resonator. The increased dissipation is due to the uneven spatial distribution of the vibrational amplitude in two different ways. First, it is related to the partial confinement of the vibrational modes. Secondly, increased dissipation may be due to singularities in the amplitude distribution. This is the case when a few points exist where the vibration is pinned to zero inducing local logarithmic singularities. This last effect can be spectacular: a single defect can dominate the surface damping by viscous forces of a square drum.

DOI: 10.1103/PhysRevE.65.036614 PACS number(s): 43.20.+g, 47.53.+n, 46.40.Ff

I. INTRODUCTION

Objects with irregular geometry are ubiquitous in nature and their vibrational properties are of general interest. How do trees respond to wind? How do sea waves depend on the topography or geometrical structure of the coasts and breakwaters? How to explain the vibrational properties of glasses? All these questions remain largely unanswered. On the other hand, current knowledge of waves and resonators indicates that even small perturbations of a resonator geometry may strongly increase the damping of specific modes. A small change of the boundary is often used in musical instrument manufacturing and microwave technology to prevent the existence of spurious modes which are effectively damped by the choice of a suitable defect in the geometry.

This paper deals with the damping properties of resonators with irregular shapes or resonators with point defects. Our general goal is to understand which of the vibrational properties influence damping, what are the reasons, and how they are related to the resonator geometries. For this purpose, we examine several representative geometries and several damping mechanisms. Between these geometries, special attention will be given to fractal drums, as the emergence of fractal geometry has been a significant breakthrough in the description of strong geometrical irregularity [1]. For simplicity we decided to study scalar vibrations instead of vector vibrations like in electromagnetic cavities. Fractals permit us in many cases to describe approximately strong statistical irregularity. They also permit the study of physical properties of deterministic but very irregular objects [2]. In this paper, we deal with damping in fractal and nonfractal types of geometrical irregularities. The principal result is that damping is directly influenced by localization and, if present, by strong singularities of the amplitude distribution.

The three main properties of vibrating systems are their spectrum, the amplitude distribution of the harmonic excitations, and their damping, the damping being related to the first two quantities. The effect of the resonator geometry on the damping has been rarely addressed, although there exists a wide body of empirical knowledge on how to build ''good'' resonators. A good resonator is a resonator that exhibits a large quality factor. The quality factor Q_n for the nth resonance mode at frequency ω_n is the dimensionless ratio of the reactive energy E_n to the loss per cycle P_n,

$$Q_n = \frac{2\pi E_n}{P_n}. \tag{1}$$

Its value characterizes the ability of the resonator, driven by an oscillating force of frequency ω_n, to accumulate reactive energy for a given power input P_n. It also determines the lifetime Q_n/ω_n of the oscillation when no power source is present. The general question is: do geometrical irregularities play a role in the losses and if so, why?

It has been suggested that there may exist an increase in the damping of fractal resonators due to the irregular distribution in space of the vibrational amplitude [3]. There exist two types of fractal resonators. The first are mass fractal resonators [4–6], for which increased damping has been shown numerically for the so-called fracton modes in percolation clusters [6]. A second type is surface fractals such as, e.g., fractal drums or fractal cavities. To prevent the use of the term ''fractons'' in this case, their eigenmodes have been named ''fractinos'' [7]. The system is generally called a ''drum'' but a real drum is a more complex physical system which possesses two membranes and an air column between them. Here, we consider a tambourine which is an instrument with only one membrane. The increased damping of fractal acoustical cavities has been predicted by numerical computations and recently been confirmed by experiments [8]. Mathematical aspects of the study of fractal drums have been previously reported [9–12]. To our knowledge, no study has been made about the comparison of damping between fractal and nonfractal (but irregular) drums. The drum geometries are shown in Fig. 1. They range from systems with fractal and nonfractal boundary roughness to square systems with point defects. Fractal drums are created, starting from a square membrane (not shown in the figure). By applying the fractal generator shown in Fig. 1(a) to each side of the square, one obtains the fractal drum of first generation. By

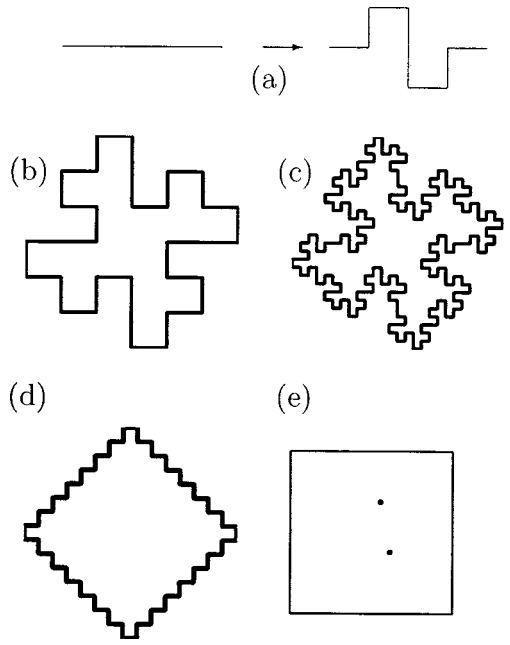

FIG. 1. (a) Generator for the prefractal geometry. (b) and (c) Fractal drum of first and second generation. The area is conserved through the iteration process. The fractal dimension of the perimeter is $D_f = \ln 8/\ln 4 = 3/2$. (d) Rough structure (nonscaling surface irregularity). (e) Example of the square system with two pinned points.

applying the fractal generator again to each straight line of the boundary structure, one can create fractal drums of arbitrary generations. In this paper, fractal drums up to the third generation are considered (the last one not being shown). Figures 1(b) and 1(c) show fractal drums of first and second generation. Figure 1(d) shows a drum with a rough, but nonscaling, boundary. The comparison of this system with the fractal drums permits us to understand the respective role of mechanical screening in hierarchical and nonhierarchical geometries. Figure 1(e) shows an example of a square membrane with point defects. In these last systems, the boundary is smooth, but the wave amplitude can develop strong singularities. In all cases we apply Dirichlet boundary conditions, which means that the vibrational amplitude is maintained at zero on the perimeter of the drum, as well as on the pinned points, shown in Fig. 1(e).

Several possible damping mechanisms are introduced in Sec. II. In Sec. III the vibrational amplitude distribution of the fundamental mode and of the fourth excited mode are described. The damping of uniform membranes is studied in Sec. IV. In Sec. V we investigate the role of the localization for the same systems. In Sec. VI we examine the case of a nonuniform membrane for which the damping force exists only at the boundary of the resonator. This can be realized by using an inhomogeneous membrane which presents large internal viscosity only at the drum periphery. Finally, in Sec. VI we study the case of a square drum with a few point defects that pin the amplitude. Contrary to the fractal drums, it is the logarithmic singularity of the amplitude distribution that creates efficient damping in this case.

II. FUNCTIONAL DEPENDENCE OF DAMPING MECHANISMS

This study is restricted to the limiting situation of weak losses. In this case the eigenmodes and eigenvalues can be reasonably approximated by those of the corresponding zero loss system. The time-dependent vibrational elongation of a given eigenstate is $z_n(x,y,t) = A_n \Psi_n(x,y)\cos(\omega_n t)$ where A_n is an arbitrary prefactor of the vibrational amplitude. The eigenstate $\Psi_n(x,y)$ is the normalized amplitude of the eigenmode of frequency ω_n which satisfies the Helmholtz eigenvalue equation:

$$\Delta \Psi_n = -\frac{\omega_n^2}{c^2}\Psi_n, \tag{2}$$

where c is the sound velocity of the membrane.

Calling ρ the surface density of the membrane, the values of the maximum elastic energy or kinetic energy E_n are

$$E_n = A_n^2 \int dxdy \frac{\omega_n^2 \rho}{2}\Psi_n^2(x,y) = \frac{A_n^2 \omega_n^2 \rho}{2}. \tag{3}$$

We use the normalization condition $\int dxdy \Psi_n(x,y)^2 = 1$. The loss per cycle is equal to the work $F_d(x,y)dz$ over one period of the damping force $F_d(x,y)$

$$P_n = \int_{\text{period}} dt \int_{\text{drum}} \left| \frac{dz_n}{dt} dF_d \right|. \tag{4}$$

Different situations exist, depending on the nature of the damping forces and hence on their spatial distributions. The damping force on an element $dxdy$ will be a function of velocity and shape of the membrane under motion. The shape dependence of the damping force can be generally expressed as a function of various space derivatives of the vibrational amplitude:

$$|dF_d| = dxdy\left[K_1 \left| \frac{dz_n}{dt} \right| + K_2 \left| \nabla \frac{dz_n}{dt} \right| \right. \tag{5}$$

$$\left. + K_3 \left(d \left| \frac{d^2 z_n}{dx^2} + \frac{d^2 z_n}{dy^2} \right| / dt \right) + \cdots \right]. \tag{6}$$

The first term characterizes a damping force proportional to the local velocity of the membrane. It describes an artificial situation where a massive membrane is linked to many individual dashpots with negligible inertia. Additionally, such a term would participate in radiation damping. A crude (and insufficient) approximation for this is acoustic radiation in a fluid, where each surface element $dxdy$ behaves as a piston. The problem of acoustic radiation in air is extremely complex for two reasons. First, if the membrane is light, its motion is strongly coupled to the air and the system does not obey a simple Helmholtz equation [13]. Second, even for a massive membrane, one should consider not only the so-called radiation monopole, but also the various multipolar radiations [14]. This is possibly important for this study, where the amplitudes exhibit singularities on every wedge of

the boundary. For simplicity we do not consider these complex effects, assuming that they can be neglected as compared to the other damping mechanisms. Then, the force on an element $dxdy$ takes the simple form $dF_1 = -dxdyK_1(dz_n/dt)$ and the value of P_n is $P_{1,n} = A_n^2 \pi K_1 \omega_n$.

The second term is proportional to the gradient of the local membrane velocity. It corresponds, for example, to damping due to the viscosity of an embedding fluid [6]. If the fluid above and below the membrane is pushed by the membrane's displacement, its vertical velocity will depend on x and y. There will exist a gradient in the fluid velocity and an associated viscous force and dissipation. Here the damping is due to a vertical viscous force of the form $dF_d = -dxdyK_2\nabla(dz_n/dt) \quad = dxdyA_nK_2\omega_n \sin(\omega_n t)\nabla\Psi_n(x,y)$. The amplitude gradient $\nabla\Psi_n(x,y)$ is the strain of the membrane. The energy loss per cycle in this case is $P_{2,n} = \pi A_n^2 K_2 \omega_n \int\int dxdy|\Psi_n \nabla\Psi_n|$. The damping depends on the spatial distribution of the vibration and strain and thus on the geometry of the drum.

The third term describes damping due to internal viscosity if the membrane is viscoelastic. Owing to its finite thickness, the upper part of the membrane is slightly more stretched than the lower part. In this case the upper layer moves relatively to the lower layer. As these layers slide, there exists a viscous force which dissipates energy. The relative horizontal displacement is proportional to the curvature $|d^2z_n/dx^2 + d^2z_n/dy^2| = |\Delta z|$. It is also proportional to the membrane and thickness [15]. The energy loss per cycle in this case is

$$P_{3,n} = \pi A_n^2 K_3 \omega_n \int\int dxdy \left| \Psi_n \left(\frac{d^2\Psi_n}{dx^2} + \frac{d^2\Psi_n}{dy^2} \right) \right|. \quad (7)$$

There is a fourth interesting situation where the damping force is nonlinear. We consider here a damping force proportional to the square of the velocity gradient $dF_d = -dxdyK_{NL}(\nabla(dz_n/dt))^2$. In that case the dissipated power can be written $P_{NL,n} = \pi A_n^3 K_{NL} \omega_n^2 \int\int dxdy \times|\Psi_n|(\nabla\Psi_n)^2$. It will be proportional to the third power of the amplitude and the quality factor will decrease when the amplitude increases. As shown below, this damping is directly related to localization as in the case of linear damping in fractal acoustical cavities.

The quality factors corresponding to these different cases can be written as (with $dV = dx\,dy$)

$$Q_{1,n} = \frac{K_1' \times \omega_n}{\int\int dV \Psi_n^2}, \quad (8)$$

$$Q_{2,n} = \frac{K_2' \times \omega_n}{\int\int dV |\Psi_n \nabla\Psi_n|}, \quad (9)$$

$$Q_{3,n} = \frac{K_3' \times \omega_n}{\int\int dV |\Psi_n||(d^2\Psi_n/dx^2 + d^2\Psi_n/dy^2)|}, \quad (10)$$

$$Q_{NL,n} = \frac{K_{NL}' A_n^{-1}}{\int\int dV |\Psi_n|(\nabla\Psi_n)^2}. \quad (11)$$

The constants K_1', K_2', K_3', and K_{NL}' represent damping factors which depend on the specific system and its material properties. For simplicity, they are assumed to be frequency independent.

III. NUMERICAL CALCULATIONS OF THE EIGENMODES

In the following sections we compare the quality factors for the different geometries of Fig. 1 and for the different damping mechanisms from Eqs. (8)–(11). To the latter we refer to as ''case 1'' until ''case 4''—damping. For the calculations, it is necessary to know the frequency spectrum ω_n and the spatial distribution of the modes amplitudes Ψ_n. These computations have been performed using the exact correspondence between the Helmholtz and diffusion equations described in [7].

Wave form singularities are expected to appear at the irregular resonator boundary. The singularities create a local augmentation of the spatial derivatives and consequently a corresponding local increase of the energy losses along the boundary [4,13]. Modes may be singular near the wedges of the boundary, i.e., their derivatives are infinite at particular points on the surface geometry. Consider, for example, a region of the membrane around a ''salient'' corner, i.e., a corner with an opening angle of $3\pi/2$ [3]. Close to the boundary, the amplitude of the vibration is very small and $\Delta\Psi$ is close to 0. In this case, using polar coordinates (r,φ) around the corner, the solution of the Laplacian with Dirichlet boundary conditions is approximately of the form

$$\Psi \sim \left(\frac{r}{r_0} \right)^{2/3} \sin(2\varphi/3), \quad (12)$$

where r_0 is of the order of the local small scale of the irregular geometry. For a fractal drum r_0 is of the order of the small cut-off scale of the fractal. The gradient $\partial\Psi/\partial r \sim r^{-1/3}$ tends to infinity when r tends to 0 [3]. This corresponds to a local infinite stress and strain of the membrane. Such a property should be true around every salient point in the structure.

Note that real physical objects only present rounded wedges. Around these wedges, the derivative does not tend to infinity but to a large finite value proportional to the inverse of the curvature radius of the contour.

Due to the existence of singularities, precise eigenfunctions are required. The method described in [7] was chosen because it allows for the large spatial resolution required for the study of fractal resonators. The computation is made on a discretized square grid with lattice distance a. The 200–300 lower modes have been computed and are studied here. The states are given by their numerical values at sites i,j of the square grid, normalized by the relation

$$a^2 \sum_{i,j} \Psi_n^2(i,j) = 1. \quad (13)$$

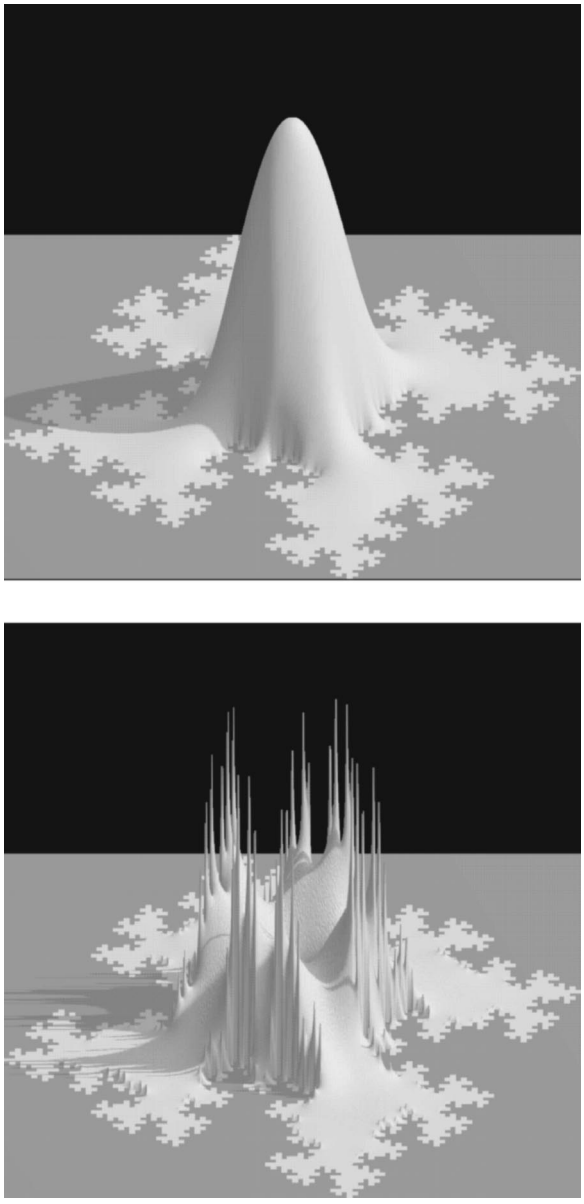

FIG. 2. Fundamental mode $n=1$. Top: Distribution of the amplitude. Bottom: Distribution of the absolute value of the strain or amplitude gradient. One observes strain peaks at the salient edges, but the edges situated in the bays are partially screened and see smaller strains. Courtesy of J. F. Colonna.

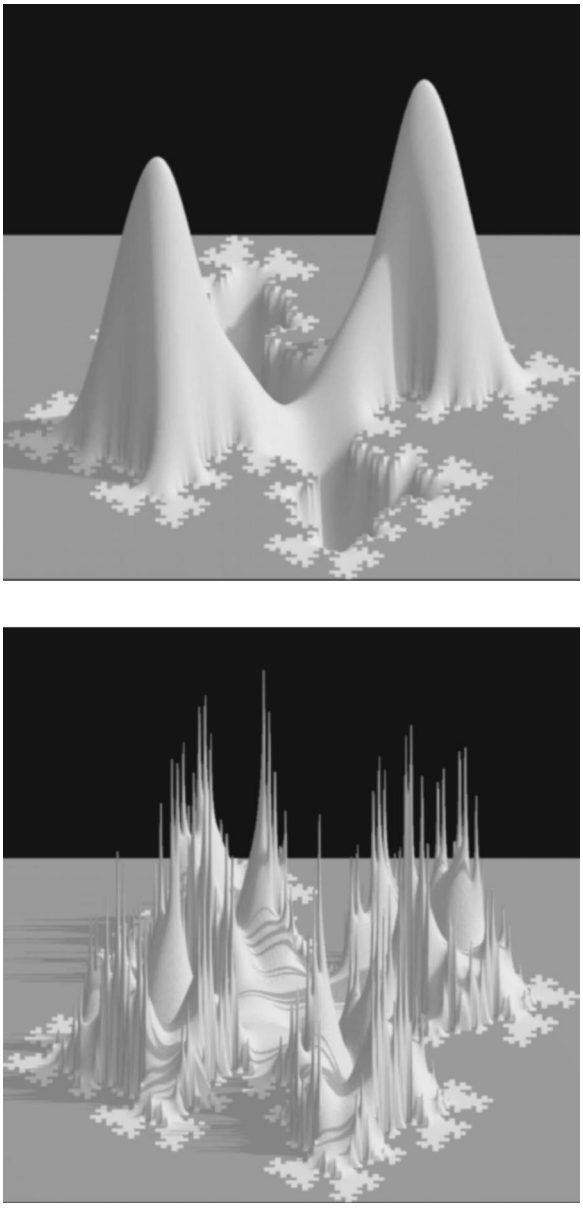

FIG. 3. Mode $n=4$. Top: amplitude distribution. Bottom: distribution of the absolute value of the strain or amplitude gradient. At higher frequency, because of the smaller wavelength, the modes penetrate more deeply into the narrower regions close to the boundary and the strain peaks are more uniformly distributed. Courtesy of J. F. Colonna.

As indicated by Eqs. (8)–(11), the Q values depend directly on the spatial distribution of the eigenfunctions and their gradients. The vibration distribution is shown for states $n=1$ and $n=4$ in Figs. 2 and 3. One can observe that the modes are singular near the wedges of the boundary, i.e., their derivatives are infinite at particular points on the surface. The fundamental state is localized in the large central region of the drum. It decays very rapidly when entering narrow regions [7]. Second, the absolute value of the gradient is smaller in narrower regions. This is caused by the decrease of the amplitude itself. The decrease of the gradient corresponds to a screening effect analogous to Laplacian screening. For Laplacian screening, the region with large Laplacian fields (here $\nabla\Psi_n$) has a dimension equal to 1, independently of the geometry [16–18]. This means that large strains are distributed over a region of total size on the order of the system size, independently of structure.

For state $n=4$ the same properties are found. However, due to the higher frequency and shorter wavelength, the mode penetrates into narrower regions, allowing for a better exploration of the geometry. If the damping really depends on wedge singularities, it should increase at high frequency.

IV. UNIFORMLY DISTRIBUTED DAMPING: RESULTS AND DISCUSSION

The quality factors are computed using the discretized expressions of the integrals (A1)–(A3) given in the Appen-

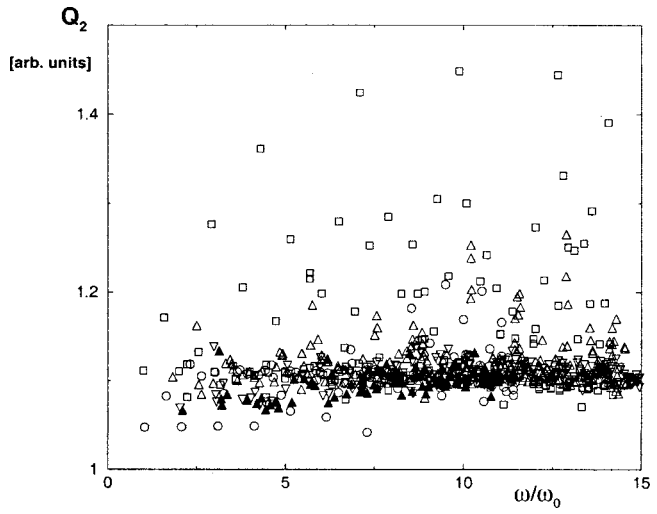

FIG. 4. Q_2 in arbitrary units for homogenous linear damping of type 2 in different geometries plotted versus the normalized frequencies ω/ω_0. The symbols represent, respectively, squares for the square initiator, empty triangles ($\triangle$) for the fractal drum of first generation, empty triangles ($\triangledown$) for the generation 2, filled triangles ($\blacktriangle$) for generation 3, and circles for the rough structure. There exists an effect of the geometry but this effect is weak and does not change the order of magnitude of the Q factor.

dix. Herein, the numerical results correspond to the same discretization grid and can thus be compared. Consider a square lattice of side L, with fundamental mode frequency $\omega_0=\sqrt{2}\pi c/L$. The area of the membrane is conserved by applying the fractal generator, which allows us to compare fractal drums of different geometries but with the same surface L^2. In the following, all frequencies are given by the size-independent normalized frequencies ω_n/ω_0. This enables us to discuss the results on a single frequency-scale. The different types of viscous damping behave in the following way.

$Q_{1,n}$ is equal to $\omega_n \rho K_1'$, independently of the spatial distribution of the vibration. In this case the quality factors depend on the frequency but are independent of the shape. Therefore, $Q_{1,n}$ is the same for vibrations in Euclidean and fractal systems (apart from the fact that the spectrum ω_n is different). Note that the same result would be obtained for the quality factor of an irregular superconducting microwave cavity in the case where damping is only due to dielectric losses in the volume of the cavity.

The values $Q_{3,n}$ are obtained from Eqs. (2), (10), and (13). One obtains $Q_{3,n}=K_3' \times c^2(\omega_n \int\int dxdy \Psi_n^2)^{-1}=K_3' c^2/\omega_n$, also irrespective to the drum shape. The fact that $Q_{1,n}$ and $Q_{3,n}$ are independent of the shape has been verified numerically.

The cases of interest are therefore case 2 (where the energy losses are due to the viscosity of the embedding fluid) and case 4 (nonlinear damping). Case 2 is computed using expressions (9) and (A1) (see the Appendix). The results are shown in Fig. 4. One can see that the Q_2 factors are modified by the irregularity of the drum but the effect remains small. This is due to the fact that the local losses are proportional to the product of the amplitude gradient with the amplitude itself. Around a wedge, the losses behave as $\Psi(r,\varphi)\nabla\Psi(r,\varphi)\sim r^{2/3}r^{-1/3}=r^{1/3}$, which means that although the strain is singular, the losses are not. Therefore, the existence of wedges in the structure does not influence the quality factors Q_2 significantly. In order to increase the damping it would be useful to prevent screening by keeping singular wedges exposed to a large strain. It is for that purpose that the rough drum has been studied (open circles in Fig. 4). Indeed, one observes that a nonscaling (or ''regular irregular'') structure is more efficient in decreasing the Q_2 factor than the self-similar geometry. The effect, however, remains small.

Therefore, it is necessary to check the numerical errors of our calculations. This can be done by comparing the numerical with the theoretical Q factor which can be computed analytically for a particular case. The fractal drum of generation ν is constituted by a collection of joint identical squares of size $L/4^\nu$. Therefore, there exists a number of trivial eigenfunctions of the form $\Psi(x,y)=\sin(2^{2\nu}m\pi x/L)\times\sin(2^{2\nu}m'\pi y/L)$ with $m,m'=1,2,3,\ldots$. For the state $(m,m')=(1,1)$ of the first-generation fractal drum, we find the numerical and analytical quality factors to be $Q_{(\mathrm{num.})}=17.755\,86$ and $Q_{(\mathrm{anal.})}=17.756\,97$. This corresponds to a numerical error of only 0.006%, far smaller than the effects discussed here, of the order of tens %. Note that, because of the finite discretization of the mesh, the wedge strain is finite. In first approximation, it corresponds to the real boundary gradient if the wedges were rounded to the scale of the mesh, here $L/128$, as explained in the preceding discussion.

The nonlinear viscous damping (case 4) is computed using expressions (11) and (A3) (see Appendix) and the results are shown in Fig. 5. The factor Q_{NL} is now strongly modified by the contour irregularity (note the logarithmic scale for Q_{NL}). Specifically, higher-order drums possess many modes with very small Q_{NL} values. One also observes that modes with close frequencies may have very different quality factors spreading over nearly one order of magnitude. The differences between the second- and third-order drum are not significant in the frequency range under study.

The fact that Q_2 and Q_{NL} show very different frequency dependencies as well as the dispersion of Q_{NL} values can be understood by considering the spatial dependence of the amplitude and the effect of mode localization. This is discussed in the next section.

V. ROLE OF THE LOCALIZATION AND FREQUENCY DEPENDENCE OF THE QUALITY FACTOR

Localization has already been found both numerically and experimentally in fractal acoustical cavities and in fractal drums [8,18]. The localization of a mode n is usually characterized by the value of its localization volume defined by

$$V_n=\frac{1}{\int \Psi_n^4(x,y)dxdy}, \tag{14}$$

where Ψ_n is normalized in the resonator volume according

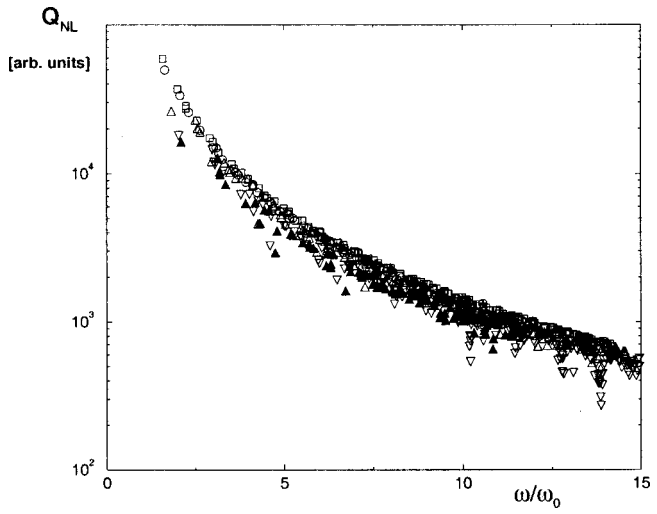

FIG. 5. Q_{NL} in arbitrary units for homogenous nonlinear damping in different geometries plotted versus the normalized frequencies ω/ω_0. The symbols represent, respectively, squares for the square initiator, empty triangles ($\triangle$) for the fractal drum of first generation, empty triangles ($\triangledown$) for the generation 2, filled triangles ($\blacktriangle$) for generation 3, and circles for the rough structure. (The same symbols as in Fig. 4.) There exists a strong effect of the frequency and of the geometry. One observes that in the same frequency range the fractal drums exhibit a large dispersion of the Q factors. This is due to very different localization effects, as shown in Sec. IV.

to Eq. (13). The relative localization volume V_n/L^2 (or participation ratio) measures the relative ''volume'' occupied by this mode.

Figure 6 shows the different localization volumes V_n/L^2 computed from the amplitude distributions. The states are

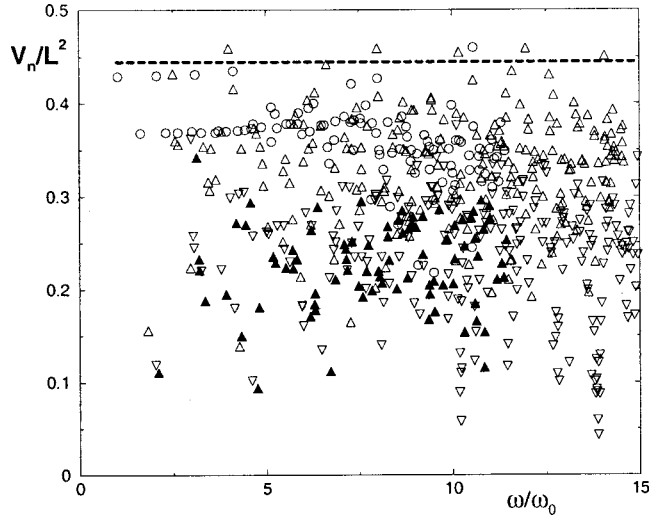

FIG. 6. Dispersion of the relative localization volume V_n/L^2 for the resonators shown in Fig. 1. The states are indexed by their normalized frequencies ω/ω_0 for all systems. The constant value $V_n/L^2=4/9$ for the square drum is indicated by the dashed line. The symbols correspond respectively: empty triangles ($\triangle$) to the fractal drum of first generation, empty triangles ($\triangledown$) to the generation 2, filled triangles ($\blacktriangle$) to generation 3, and circles to the rough structure.

indexed by their normalized frequencies ω/ω_0 and the different symbols refer to different geometries. The cloud of points in this figure are indicative of the wide dispersion of the participation ratios, first, between different systems and second, also for a given system. Only for the square drum, where the eigenstates are delocalized sine functions, $V_n/L^2=4/9\approx 0.44$ for all states. The relative localization volumes of the second (triangles down) and the third-order drum (filled triangles) are distributed between 0.05 and 0.35. These values reflect a very different behavior of the corresponding modes. The upper values are not very distinct from the value of a regular square drum and accordingly, the respective wave functions are more or less distributed over the whole system. The modes that are significantly more confined than $V_n/L^2\approx 0.3$, are called ''localized.'' Most interesting are the modes with values of less than 0.1. We can see in the figure that there are several of them that occur in branches around special frequencies. Examples are the modes around $\omega/\omega_0=10$ and 14 for the second-order drum. It is exactly those modes which show the smallest Q_{NL} factors in Fig. 5. A different behavior is found for the rough drum (circles). Its localization volumes (above 0.3) indicate that its vibrations are not localized, as expected as this resonator possesses no screened regions. The following discussion permits us to relate in a formal manner the observed dispersion in Fig. 5 to the observed dispersion in Fig. 6 linking directly damping and localization.

Using V_n one can obtain a rough estimate of the quality factors by distinguishing between regions of large and small amplitude. We consider the regions of large amplitude and define an average absolute amplitude by $\langle|\Psi_n|\rangle \equiv V_n^{-1}\int dxdy|\Psi_n|$. For a localized mode, assuming that the amplitude is approximately zero outside its localization volume, one can write the normalization condition as $\langle|\Psi_n|\rangle^2 \times V_n\sim 1$ or

$$\langle|\Psi_n|\rangle\sim(V_n)^{-1/2}. \tag{15}$$

We now consider the different types of damping separately, according to cases 2 and 4. At frequency ω_n the characteristic distance for the amplitude space variation is a half-wavelength $\lambda_n/2=\pi c/\omega_n$. The order of magnitude of the gradient $\nabla\Psi$ is $2\langle|\Psi_n|\rangle/\lambda_n=V_n^{-1/2}\omega_n/\pi c$, which leads to a $Q_{2,n}$ factor of

$$Q_{2,n}\sim\omega_n\Big/\int dV|\Psi\nabla\Psi|\sim(V_n)^0\times(\omega_n)^0. \tag{16}$$

This semiquantitative prediction means that $Q_{2,n}$ is essentially independent of frequency and localization, which is compatible with the data in Fig. 2 where we found that the effects of geometry are relatively small.

The situation is very different for the nonlinear damping, where we find by the same estimations that $Q_{NL,n}$ is of the form

$$Q_{NL,n}\sim 1\Big/\int dV\Psi_n(\nabla\Psi)^2\sim(V_n)^{1/2}\times(\omega_n)^{-2}. \tag{17}$$

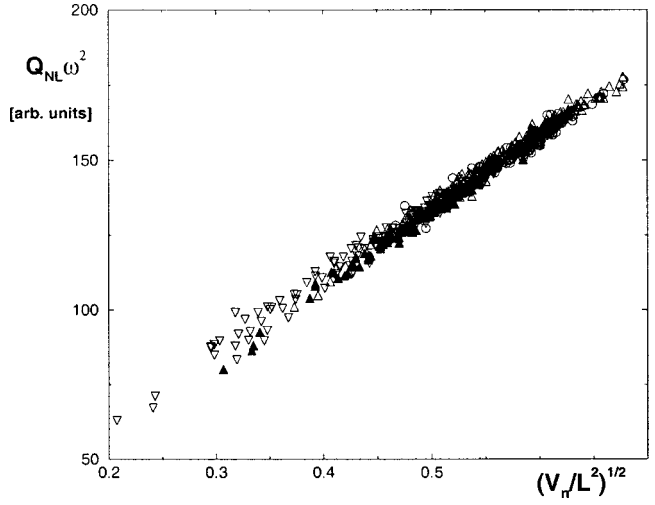

FIG. 7. $Q_{NL}\omega^2$ in arbitrary units versus $(V_n/L^2)^{1/2}$ for all systems, including the square generator. Same symbols as in Fig. 4. Note that the vertical scale is linear whereas the scale on Fig. 5 is logarithmic.

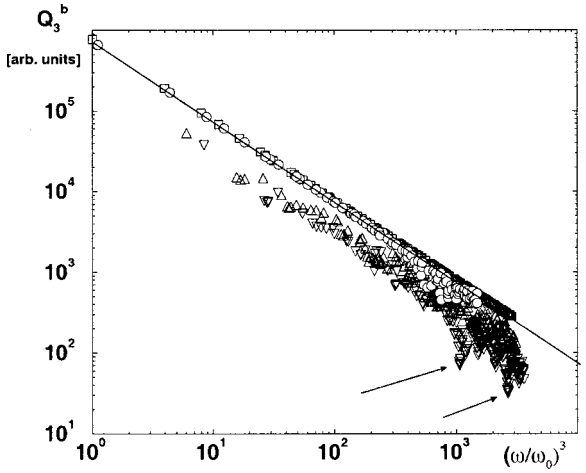

FIG. 8. The quality factor Q_3^b in arbitrary units versus $(\omega_n/\omega_0)^3$ for the boundary linear damping of type 3 with the same symbols as in Fig. 4. The line of slope -1 is a guide to the eye. For the second-order drum, the states with frequencies around $\omega/\omega_0 \approx 10$ and $\omega/\omega_0 \approx 14$, showing strong localization and very small quality factors, are indicated by arrows.

The localization argument indicates that Q_{NL} should be markedly smaller for localized states and high frequencies. This is verified in Fig. 7 where the relation (11) is compared to the numerical results. The values of $Q_{\mathrm{NL}}\omega^2$ are plotted versus $(V_n/L^2)^{1/2}$. The fact that for all drums and all states the points fall onto the same universal curve illustrates that damping is directly influenced by localization and that the simple semiquantitative reasoning described above applies to irregular drums, independent of their shape. Note the linear scale in the figure.

For all these cases, the divergences of the strain at salient points do not contribute significantly to the dissipation. Even for the nonlinear case, the local strain diverges as $\partial\Psi/\partial r \sim r^{-1/3}$ and the integrand is of the form r^1 which is regular. Again, damping due to uniformly distributed mechanisms is not dominated by strain divergences.

VI. BOUNDARY DAMPING

In the last two sections we study cases where the dissipation mechanism is not distributed uniformly over the membrane. In the first case of practical interest, only the periphery of the drum presents internal viscosity (case 3). The membrane is purely elastic in the drum interior and viscoelastic along the boundary of the resonator. This situation is of practical interest when one wishes to dampen spurious high frequency resonances of membranes. It is linear damping described by Eq. (A2) but the integration has to be performed only over a small layer along the boundary. We call the quality factor Q_3^b.

The power $P_{3,n}$ dissipated along the boundary can be written from Eq. (7) as

$$P_{3,n} = \pi A_n^2 K_3 \omega_n \sum_{\text{boundary}} |\Psi_n(a)||\Delta\Psi_n(a)|, \qquad (18)$$

where $\Psi_n(a)$ and $\Delta\Psi_n(a)$ are the respective values of the amplitude and of the Laplacian on mesh sites next to the boundary, i.e., at a distance a of one lattice constant. The data corresponding to the fractal drum of third generation are not given due to the lack of resolution of the smaller cutoff in the grid used for the computation (only three vibrating sites). The other results are shown in Fig. 8, where Q_3^b is plotted versus $(\omega/\omega_0)^3$. One observes (i) a strong decrease with frequency following a power law with exponent -3, (ii) a gradual decrease of the quality factors as one moves from regular to more and more irregular drums, and (iii) a strong effect of the localization. So, the quality factors for the square and the rough drums, which show no localization, lie clearly above those of the fractal drums, which have many localized states. Additionally, for the second generation, those states with frequencies around $\omega/\omega_0 \approx 10$ and $\omega/\omega_0 \approx 14$, showing strong localization, have the smallest quality factors (indicated by arrows in Fig. 8).

The general behavior of the results may be understood as follows: with $|\Delta\Psi_n| \sim \omega_n^2 |\Psi_n|$, one expects that

$$Q_3^b \sim 1 \Big/ \left(\omega_n \sum_{\text{boundary}} \Psi_n^2(a) \right), \qquad (19)$$

where the sum runs over all boundary sites. The value of the sum in Eq. (19) depends on the amplitude distribution and the localization close to the boundary. (Note that the square and the rough generator show no localization.) If the amplitudes behave approximately as sine waves, the amplitude value next to the boundary is proportional to (a/λ) and thus to ω_n. It is also proportional to the amplitude factor $\langle|\Psi_n|\rangle \sim (V_n)^{-1/2}$ of Eq. (15) which depends on localization. This means that $Q_3^b \sim (\omega_n \langle \Sigma'_{n,b} |\Psi_n|\rangle^2)^{-1} \sim (V_n) \times (\omega_n^3 \Sigma_{n,b} 1)^{-1}$, where the prime denotes the "active boundary" and the sum $\Sigma'_{n,b}$ runs over all boundary sites in the localization regions of mode n.

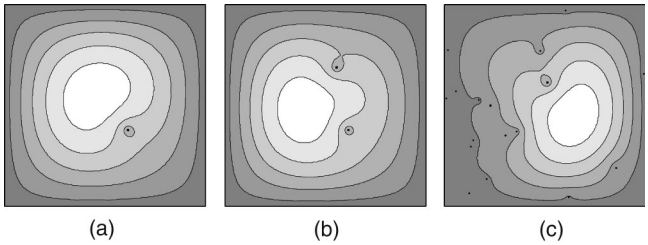

FIG. 9. Fundamental modes of square systems with (a) one, (b) two, and (c) 20 pinned points. The amplitudes are indicated by different gray levels. The white regions stand for very large amplitudes. The darker tone stands for nearly zero amplitude. (Node lines do not exist in the fundamental mode.)

This argument, which is valid for all the structures, explains the frequency power law. The interpretation of the dependence of Q_3^b on the localization, on the other hand, is difficult, because Q_3^b depends both on the localization volume and on the set of perimeter sites which are ''active'' in the localization volume. Also, the local irregularity around wedges could play a role as its relative contribution to damping effects could be larger than in the case of homogeneous damping. To disentangle these various factors would require the computation of the eigenmodes of fractal drums of higher generations with sufficient resolution. This is currently not possible.

In any case, if one wishes to increase the damping by the singular behavior of the strain, one should search for a stronger divergence around salient points. This is found around needles where Ψ behaves as $r^{1/2}$ and $\nabla\Psi$ therefore as $r^{-1/2}$. Even in that extreme case the integrands for the various integrals mentioned above are regular and the singularities of the geometry play only a small role. In contrast, the existence of pinned points inside a regular drum will create logarithmic singularities which might dominate the damping. This is shown in the next section.

VII. DAMPING AROUND PINNED POINTS

We discuss here the damping of a regular square drum on which a certain number of inner points are pinned. One example is shown in Fig. 1(e). The vibrational amplitude vanishes at these points and the membrane is viscoelastic along the boundary as well as around the pinned points. We consider three different cases, whose fundamental modes are shown in Figs. 9(a)–9(c). It can be seen that around pinned points, there are large gradients of the vibrational amplitudes. The choice of the positions for the pinned points was guided by the effort to avoid the natural nodelines caused by the symmetry of the square.

In case (a), only one point is kept fixed at a position close to $(x,y)=(L/R,L-L/R)$, where R is the golden mean. The use of the golden mean is in order to place the pinned point at the most ''antiharmonic'' location with regard to the horizontal and the vertical symmetry axes of the membrane. R is most distant from a rational number and so no nodelines of the sine functions $\sin(n\pi x/L)$ can occur close to $x=RL$ or $x=(1-R)L$. However, this point lies close to a diagonal which is also a symmetry axis. Eigenstates must be either symmetric or antisymmetric under reflexion on the diagonal. The antisymmetric modes of the square have a zero value on the diagonal. These modes are unperturbed by the existence of a pinned point on this diagonal. In order to suppress any symmetry in case (b) two pinned points were introduced at the positions $(x,y)=(L/R,L-L/R)$ and $(x,y)=(L/4+L/(2R),L-L/(2R))$. In case (c) 20 randomly chosen points are pinned.

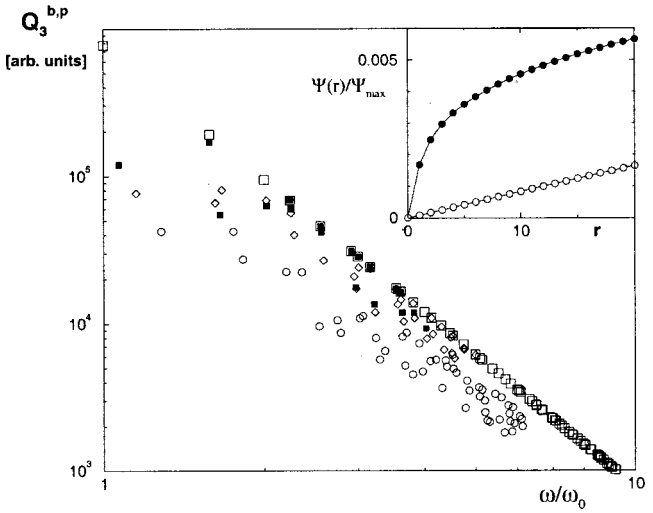

FIG. 10. $Q_3^{b,p}$ in arbitrary units for square membranes with different numbers of pinned points, plotted versus the normalized frequencies ω/ω_0. The different symbols represent the normal square without pinned points (open squares) and the systems of Fig. 10: (a) full squares, (b) diamonds, and (c) open circles. Inset: The wave function $\psi(r)$ is plotted against the horizontal distance r from a pinned point (filled circles) and from the boundary (open circles) for the system of Fig. 9(a). It can be recognized that $\psi(r)\sim\log r$ for $r\neq 0$ around the pinned point and $\psi(r)\sim\sin r\approx r$ at small distances from the boundary.

Now the stronger singularities in the amplitudes do modify the damping. Very close to a fixed point, the solution of the Laplace equation shows logarithmic singularities, $\psi(r)\sim\log r$, and one expects large contributions to damping at small r. In that case the sum in Eq. (19) contains large $(\log a)^2$ terms at the denominator. The numerical results are shown in Fig. 10. The figure contains the data for the normal square without pinned points and for the systems of Figs. 9(a)–9(c). In the inset, the behavior of the vibrationonal amplitudes $\psi(r)$ are shown along the horizontal distances r from the pinned point of system 9(a) and from the boundary. The singularity around the pinned point is observed. Close to the regular boundary, on the other hand, the amplitude behaves linearly as $\sin r\sim r$. The value of $\psi(r)$ at a distance of one lattice constant from a pinned point is about 20–30 times larger than at the same distance from the boundary. Consequently, in a square lattice of side length $L=256a$, one single pinned point is about five times more efficient for the damping than all the approximately 1000 boundary points altogether. (This estimation contains the difference in ψ^2 and the number of neighbors around the pinned point and would

be even larger if we considered viscoelasticity up to second-nearest neighbors.)

As one observes in Fig. 10, the quality factors decrease drastically due to the existence of pinned points. As expected, for one pinned point on the diagonal [Fig. 9(a)] the quality factor for the fundamental is decreased by a factor of about 5. It is a most remarkable result that a single point defect can dramatically increase the damping. It has to be put in relation with a common technique in radar technology, where a small wire is introduced into a microwave cavity at a maximum of the electric field of an eigenmode in order to ''kill'' that mode. Note that damping in microwave cavities is also a surface damping due to the classical skin effect.

However, the modes that are antisymmetric with respect to the diagonal are unperturbed and show the same quality factors as the square. The symmetry effect is suppressed in the systems with several pinned points. In case (b) or (c) there are always several pinned points close to amplitudes maxima—at least at low frequencies [cf. Fig. 10(c)]. Therefore, in the entire low-frequency regime, the quality factors $Q_3^{b,p}$ are strongly diminished as compared to the boundary damping in the normal square. With increasing frequency, the relative effect becomes smaller, because modes become more and more confined between defects. At the same time the frequency spectrum shifts to higher values. Contrary to the results of the fractal drums, the states of these membranes are not strongly localized. The participation ratios of these modes are found to be $V_n/L^2 \geqslant 0.3$, much larger than for the fractal drums. Therefore the observed damping is, in this case, a direct consequence of the singular behavior of the vibration amplitudes. Not shown here, we have computed the damping of the fundamental state for one single pinned point with coordinates $(x, L/2)$ as a function of x. A first order perturbation theory correction would predict that the losses go with $\sin^2(\pi x/L)$ attached to the unperturbed state. This is approximately found.

VIII. CONCLUSION

In summary it has been shown that irregular shapes not only drastically alter the spatial character of drum vibrations but may also increase their damping. This has been investigated for several geometries (with scaling and nonscaling surface roughness and with pinned point defects) and for different damping mechanisms. The general conclusion is that irregularity increases the effective damping of the vibration. It has been found that there are two different reasons for these effects: localization and the existence of algebraic singularities of the spatial distribution of the modes amplitudes.

For drums without point defects the damping is related directly to localization as a localized vibration presents larger amplitude and velocity gradients and therefore increased dissipative viscous forces. On the other hand, the existence of a few pinned points on an otherwise regular drum can increase the damping dramatically. This is due to the existence of logarithmic singularities in the viscoelastic behavior around pinned points. For example, it has been found that only 2 pinned points suitably placed are significantly more efficient in damping than some 1000 points along the smooth boundary. This last damping phenomena is not related to localization, but to the strong singularity of the vibrational amplitude. This is the first quantitative explanation of why point defects, such as those used in radar technology, really permit the ''kill'' of unwanted spurious modes.

ACKNOWLEDGMENTS

We would like to thank Jean-Francois Colonna for providing us with Figs. 2 and 3 and Markus Dejmek and Armin Bunde for a careful reading of the manuscript and for interesting remarks. One of us (S.R.) has benefited from the E.E.C. program ''Human Capital and Mobility.'' The computation was performed at the ''Institut du Developpement et des Ressources en Informatique Scientifique'' (IDRIS) in Orsay, France. CNRS is unite mixte du CNRS No. 1254.

APPENDIX

With the notations of the discretized lattice the integrals in Eq. (9) are substituted by the expression

$$\int\int dxdy|\Psi_n\nabla\Psi_n| = (a^2/2)\sum_{i,j} |\Psi_n(i,j)|[|\Psi_n(i+1,j)-\Psi_n(i,j)| + |\Psi_n(i-1,j)-\Psi_n(i,j)| + |\Psi_n(i,j+1) - \Psi_n(i,j)| + |\Psi_n(i,j-1)-\Psi_n(i,j)|]. \quad \text{(A1)}$$

In the same way the integrals in Eqs. (10) and (11) are expressed on the discretization grid as

$$\int\int dxdy\Psi_n|(d^2\Psi_n/dx^2)+(d^2\Psi_n/dy^2)| = a^2\sum_{i,j} |\Psi_n(i,j)|[|\Psi_n(i+1,j)+\Psi_n(i-1,j)-2\Psi_n(i,j) + \Psi_n(i,j+1)+\Psi_n(i,j-1)-2\Psi_n(i,j)|], \quad \text{(A2)}$$

$$\int\int dxdy|\Psi_n|(\nabla\Psi_n)^2 = (a^2/2)\sum_{i,j} |\Psi_n(i,j)|[|\Psi_n(i+1,j) - \Psi_n(i,j)|^2 + |\Psi_n(i-1,j) - \Psi_n(i,j)|^2 + |\Psi_n(i,j+1) - \Psi_n(i,j)|^2 + |\Psi_n(i,j-1) - \Psi_n(i,j)|]^2. \quad \text{(A3)}$$

[1] B. B. Mandelbrot, *The Fractal Geometry of Nature* (Freeman, San Francisco, 1982).
[2] B. Sapoval, *Fractals* (Aditech, Paris, 1990); *Universalités et Fractales* (Flammarion, Paris, 1997).
[3] B. Sapoval, Physica D **38**, 296 (1989).
[4] S. Alexander and R. Orbach, J. Phys. (France) Lett. **43**, L625 (1982).
[5] T. Nakayama, K. Yakubo, and R. Orbach, Rev. Mod. Phys. **66**, 381 (1994).
[6] S. Russ and B. Sapoval, Phys. Rev. Lett. **73**, 1570 (1994); in *Dynamics in Small Confining Systems*, edited by J. M. Drake, S. M. Troian, J. Klafter, and R. Kopelman, MRS Symposia Proceedings No. 366 (Materials Research Society, Pittsburgh, 1995), p. 243; Nuovo Cimento D **16**, 1103 (1994).
[7] B. Sapoval, T. Gobron, and A. Margolina, Phys. Rev. Lett. **67**, 2974 (1991); B. Sapoval and T. Gobron, Phys. Rev. E **47**, 3013 (1993); S. Russ, B. Sapoval, and O. Haeberlé, *ibid.* **55**, 1413 (1997).
[8] B. Sapoval, O. Haeberlé, and S. Russ, J. Acoust. Soc. Am. **102**, 2014 (1997); B. Hébert, B. Sapoval, and S. Russ, *ibid.* **105**, 1567 (1999).
[9] M. L. Lapidus and M. Pang, Commun. Math. Phys. **172**, 359 (1995).
[10] M. Lapidus, J. W. Neuberger, R. Renka, and C. A. Griffith, Int. J. Bifurcation Chaos Appl. Sci. Eng. **6**, 1185 (1996).
[11] M. Levitin and D. Vassiliev, Proc. London Math. Soc. **72**, 178 (1996).
[12] J. Fleckinger, M. Levitin, and D. Vassiliev, Proc. London Math. Soc. **71**, 372 (1995).
[13] G. A. Kriegmann and C. S. Scandrett, J. Acoust. Soc. Am. **86**, 788 (1989).
[14] P. M. Morse and K. Uno Ingard, *Theoretical Acoustics* (Princeton University Press, Princeton, N.J., 1968).
[15] P. G. de Gennes and J. Prost, *The Physics of Liquid Crystals* (Clarendon Press, Oxford, 1995), p. 418.
[16] N. G. Makarov, Proc. London Math. Soc. **51**, 369 (1985).
[17] P. Jones and T. Wolff, Acta Math. **161**, 131 (1988).
[18] B. Sapoval, M. Filoche, K. Karamanos, and R. Brizzi, Eur. Phys. J. B **9**, 739 (1999).
[19] C. Even, S. Russ, V. Répain, P. Pieranski, and B. Sapoval, Phys. Rev. Lett. **83**, 726 (1999).